USE OF AES AND RGA TO STUDY NEUTRON-IRRADIATION-ENHANCED SEGREGATION TO INTERNAL SURFACES*

CONF-800205--15

G. R. Gessel† and C. L. White

Oak Ridge National Laboratory, Oak Ridge, Tennessee 37830

ABSTRACT

The high flux of point defects to sinks during neutron irradiation can result in segregation of impurity or alloy additions to metals. Such segregants can be preexisting or produced by neutron-induced transmutations. This segregation is known to strongly influence swelling and mechanical properties. Over a period of years, facilities have been developed at ORNL incorporating AES and RGA to examine irradiated materials. Capabilities of this system include in situ tensile fracture at elevated temperatures under ultrahigh vacuum 10^{-10} torr and helium release monitoring. AES and normal incidence inert ion sputtering are exploited to examine segregation at the fracture surface and chemical gradients near the surface. Work on irradiated stainless steels shows that this technique, coupled with scanning electron fractography, conventional and analytical electron microscopy, allow one to identify the important microstructural features affecting the observed embrittlement. The sensitivity of the AES and RGA techniques allows one to examine microchemical fluctuations that are not accessible by analytical electron microscopy.

---

*Research sponsored by the Division of Materials Sciences, U.S. Department of Energy, under contract No. W-7405-eng-26 with the Union Carbide Corporation.

†Present address: Department of Mechanical Engineering, University of Arkansas, Fayetteville, Arkansas 72701

INTRODUCTION

The effects of neutron irradiation on the properties of structural materials frequently appear to involve internal interfaces such as grain boundaries, precipitate-matrix interfaces, and internal-free surfaces (e.g., of voids and bubbles). The properties of these interfaces are likely to be strongly influenced by trace element segregation driven by both equilibrium and nonequilibrium mechanisms. The purpose of this paper is to describe the use of Auger electron spectroscopy (AES) and residual gas analysis (RGA) for the study of interfacial segregation in irradiated alloys. Experimental results on neutron-irradiated Inconel 706 (IN706) will be presented as an example of how these techniques can be applied.

BACKGROUND

The correlation between interfacial segregation and changes in mechanical properties of polycrystalline material is well documented. Reductions in both fracture stress and total elongation for tensile tests have been observed to coincide with metalloid segregation to metal interfaces. Such segregation-induced embrittlement has been reported for sulfur in nickel (1,2) and nickel base alloys (3); phosphorous in iron (4,5) and austenitic steels (6) and bismuth in copper (7). The data of Hondros and McLean (8) for the Bi-Cu

system show both the ultimate tensile strength and grain boundary energy decreasing as bulk Bi content is increased. A similar study by Joshi and Stein (7) showed that reductions in fracture stress, ultimate tensile strength and total elongation correlate well with increases in bismuth concentration at grain boundaries in bismuth-doped copper.

The usual treatment of segregation induced embrittlement begins with an expression for the work done in creating a grain boundary crack (W)

$$W = 2\gamma_s - \gamma_{Gb} + W_p + W_D \quad . \tag{1}$$

The terms in this energy audit are γ_s surface free energy, γ_{Gb}-grain boundary energy, W_p-plastic work, and W_D-miscellaneous dissipation. Thermodynamic arguments as well as experimental observations show that equilibrium segregation to an interface decreases interfacial energies. The $2\gamma_s - \gamma_{Gb}$ term represents the energy expended in reversibly producing a brittle crack. This term could be increased or decreased, as a result of segregation by some amount $\Delta\gamma$ which is the change in cohesive energy of the boundary. Since fracture ultimately means that bonds are broken, this is often converted to a change in average interfacial bond energy. This averaging approach, of course, neglects important spatial variations in bond energy. Equation (1) is also restricted to the growth of an isolated crack and therefore neglects competing processes taking place throughout the specimen. Rather modest changes in surface energy can profoundly influence other material properties. Figure 1 shows the effect of surface energy on the energy for vacancy cluster (void) nucleation (9). Nucleation rates represented there (upper curve, 2.3×10^{-6} cm^{-3} s^{-1} lower curve, 3.1×10^{9} cm^{-3} s^{-1}) span 15 orders of magnitude.

While much of the literature connecting impurity segregation with embrittlement addresses only equilibrium segregation, irradiated materials

may also experience non-equilibrium segregation. Non-equilibrium segregation results from the flux of irradiation-induced point defects to internal sinks. Enrichment or depletion of impurities or alloy constituents at sinks can occur, depending upon the type of interaction that exists between these elements and the point defects.

Figure 2 illustrates schematically three mechanisms by which non-equilibrium segregation might occur. The first case shown in Fig. 2 represents an enrichment of slower moving alloy components at a grain boundary (one type of sink) for elements diffusing by a vacancy mechanism. Case 2 addresses the case of self-interstitial diffusion and results in grain boundary enrichment of faster diffusing species. Defect-element binding is represented by case 3 which can result in grain boundary enrichment of the bound species. The current state of kinetic models for irradiation-produced segregation can be found elsewhere (10).

It is important to keep in mind that nonequilibrium segregation (by definition) occurs in opposition to thermodynamic driving forces. At some point a steady-state condition will be reached when back-diffusion (driven by equilibrium thermodynamics) will balance the nonequilibrium flux due to defect production in the lattice. It is also important to note that since equilibrium segregation tends to minimize γ_{Gb} any nonequilibrium level of segregation will cause γ_{Gb} to be greater than its minimum value.

A second effect of irradiation on segregation could be increased kinetics of equilibrium segregation. The extent of segregation at equilibrium is generally expected to increase as temperature is decreased; however, the kinetics of segregation will decrease. This competition between kinetics and thermodynamics tends to limit the extent of segregation that actually occurs at low temperatures. By increasing atomic mobility, irradiation could permit thermodynamically favorable (but kinetically limited) segregation to occur in shorter periods of time or at lower temperatures than would be possible in the absence of irradiation.

Finally, significant quantities of helium can be produced via (n,α) reactions on many alloys, especially those containing nickel. Segregation of helium to internal interfaces could have significant effects on alloy behavior. If bubbles are formed at internal boundaries, this of course would lower the load bearing cross section and facilitate localized (and hence low ductility) failure in the vicinity of the boundaries.

In all cases where solute enrichment at internal interfaces occurs, the region of enrichment is expected to be rather narrow. For the case of equilibrium segregation, solute-enriched regions are typically only a few atom layers (< 1 nm) thick. Somewhat thicker regions are often anticipated for non-equilibrium type segregation, sometimes extending several tens of nanometers from the interface plane.

When segregation occurs in a very thin region at an interface, it can be difficult to detect using conventional analytical techniques. Auger electron spectroscopy (AES) is a well-established tool for examining thin interfacial regions when they can be exposed as external surfaces. AES is sensitive to only the top few atom layers on an exposed surface because it involves detection of characteristic low-energy Auger electrons. Subsurface regions can be

exposed for analysis by sputtering with inert gas ions. Alternate AES and sputtering permit information about the depth distribution of segregated species to be obtained.

An important requirement for the use of AES to study interfacial segregation is that the interface in question must be exposed as a free surface. In the case of internal interfaces, this is normally achieved by fracturing the specimen along those interfaces. The conditions under which this fracture takes place are important and can significantly affect the interpretation of AES results. One requirement is that the fracture surface be created under ultra-high vacuum (UHV) conditions. At pressures greater than $\sim 10^{-7}$ Pa, contamination of clean surfaces occurs so rapidly that AES results are significantly affected.

One benefit of having to fracture specimens in a UHV environment is that any gas release upon fracture can be easily monitored. If a residual gas analyzer (RGA) is used, the pressure increase due to a specific gaseous species can be determined. This approach has proven useful in the past for observing helium release from irradiated specimens; however, other gaseous transmutation products could also be detected.

In the remainder of this paper we will present and discuss experimental results on neutron-irradiated Inconel 706. This alloy exhibits poor elevated-temperature ductility in postirradiation tensile tests. The failure mode in these tests is largely intergranular, suggesting the possibility that irradiation-induced or -enhanced segregation might be important.

Experimental Techniques

Figure 3 is a top view of an Auger system that has been developed over a period of years at Oak Ridge National Laboratory. Experimental studies using this system have been previously reported by Clausing and Bloom (11),

Sklad et al. (12) and White et al. (13). This system uses a cylindrical mirror analyzer with coaxial electron gun and electronics. The electron gun has a 5 μm minimum spot size and the electron beam can be rastered to provide images and elemental maps of the surface being analyzed. A normal incidence 1 kV inert ion sputter gun with movable sputter shield and a quadrupole mass analyzer are also part of the system. Not shown in Fig. 3 is a transfer-lock device into which specimens are introduced prior to entry through the specimen entry port into the main chamber.

Figure 3 also shows the location of a tensile fracture stage, described in greater detail in Fig. 4. Electrical leads are used to pass current through the specimen for elevated temperature tests. The hollow threaded pull rod and ceramic standoffs limit the specimen load to approximately 90 lb. The specimen holder (shown down-side up) together with a specimen [0.4 in. (1.016 cm) long with a 0.04 in. (1.016 mm) cross section] are shown in Fig. 5. All specimens in this work entered the system in an electropolished condition. Temperature measurements were made by sighting through the front viewing port (Fig. 3) onto the notched portion of the Auger bar with an infrared pyrometer.

Table 1 gives the composition of the IN706 used in this study. Tensile specimens of this alloy were given the following thermal treatment (955°C, 1 h/water quench/843°C, 3 h/air cool/720°C, 8 h/furnace cool to 620°C/620°C, 10 h/air cool), which we designate the STA (solution treated and aged) condition. These tensile specimens were then irradiated to a dose of 5×10^{22} n/cm^2 at 500°C. The results of tensile tests on these specimens are summarized in Table 2. When tested at 610°C, these specimens show almost

no ductility, in sharp contrast to the unirradiated alloy. There also appears to be some increase in yield strength and decrease in ultimate tensile strength associated with the irradiation.

Figures 6 and 7 compare TEM micrographs of unirradiated and irradiated IN706-STA, respectively. The unirradiated alloy (Fig. 6) is strengthened by γ' and γ'' and has a precipitate-free zone adjacent to grain boundaries which contain η phase precipitates. Figure 7 shows the microstructure of a specimen from the head of the irradiated tensile specimen T3 (Table 2). The irradiated specimen has no detectable precipitate-free zone and does have voids or bubbles at precipitate-matrix interfaces along the grain boundaries.

A notched Auger tensile specimen, A3, was cut from the gage section of failed tensile specimen, T3. The Auger specimen was fractured at approximately 610°C in the AES system and the resulting fracture surface was examined using AES. The helium partial pressure was monitored during fracture, and no release of helium was detected.

A derivative type Auger spectrum from the fresh fracture surface of specimen A3 is shown in Fig. 11. This spectrum was obtained by rastering the primary electron beam over roughly one-half of the fracture surface; and as such represents an average surface composition for that surface. In addition to the intentionally added metallic alloying elements (see Table 1), P, C and O are present in significant concentrations. An approximate* quantitative analysis

*These values are obtained by measuring the peak-to-peak intensity for each element, dividing that intensity by an elemental sensitivity factor, and normalizing these values to 100%. This does not correct for matrix effects, distribution effects, and differences in electron mean free path.

of this spectrum indicates P, C, and O levels of 5, 5, and 1 at. %, respectively. Spot analyses on this fracture surface indicated that the phosphorous concentration varied significantly, and was as high as 13 at. % in certain areas. This indicates phosphorous concentrations on the fracture surface over 600 times the average bulk concentration.

Carbon and oxygen levels indicated in Fig. 11 are also significantly greater than bulk levels. The observed carbon could arise from at least three sources: (1) elemental carbon segregated to the fracture surface, (2) carbon-rich precipitates on the fracture surface, and (3) adsorption of carbon containing residual gases (e.g., CO and CH_4) from the analysis chamber. Similar possibilities also exist for oxygen; however, it is believed that most of the oxygen observed in Fig. 11 results from contamination by residual gases.

Following the analysis of the as-fractured surface, specimen A3 was positioned in front of the inert ion sputter gun and sputter etched for 5 min. The ion current density and ion energy were adjusted to allow an etching rate of approximately one atom layer per minute. Figure 12 shows an Auger spectrum of specimen A3 after the 5-min sputter etch. Comparison of the spectra in Figs. 11 and 12 reveals that the phosphorous peak is gone. This indicates that the phosphorous-enriched zone near the fracture surface is only a few atom layers thick. This comparison will also reveal that the carbon and oxygen signals have increased. The increased carbon could be due to the "smearing" or uncovering of carbon-rich precipitates.

Figures 8, 9, and 10 show scanning electron micrographs of the fracture surface that was analyzed using AES. The failure mode in this specimen was a mixture of intergranular and transgranular modes. Figure 10 shows the small dimples that covered many of the grain boundary facets. The spacing of these dimples and the cavities in Fig. 7 are similar.

In order to determine what effect, if any, the postirradiation heating at 610°C might have had on these results, in situ heating of unirradiated IN706 foils was carried out. AES analysis of external surfaces indicated that 2–4% phosphorous can segregate to the external surface of this material when heated for 10–30 min in the temperature range 600–650°C. These observations indicate that the grain boundary fracture surfaces created by high-temperature fracture may not have the same composition as the unfractured grain boundaries in "as-irradiated" material.

In an effort to expose grain boundaries (for AES analysis) without any postirradiation heating, electrolytic hydrogen charging has been exploited. Hydrogen charging was conducted in a round bottom flask outfitted with a heating mantle, reflux condenser, and two platinum electrodes. The specimen was held in a platinum wire mesh envelope and suspended between the electrodes using platinum wire. A 4% H_2SO_4 solution containing 0.25 g/L of As_2O_3 was used for charging, and a current density of 0.1 A/cm^2 at 4 V was maintained at the specimen. In order to maximize the thickness of the hydrogen diffusion zone, temperatures close to boiling are desirable. Our work has successfully used temperatures of 85–90°C and charging times up to 72 h. Longer charging times are desirable; however, during lengthy charges a surface film periodically forms on the specimen which must be removed by electrolytic polishing to ensure free entry of hydrogen. Preliminary AES results from this effort indicate that as-irradiated boundaries contain 1–2 at. % phosphorous. Helium partial pressure was also monitored, but no helium release detected. Future experiments on hydrogen charged specimens are intended to compare grain boundary compositions for unirradiated and irradiated alloys.

Discussion

A partially intergranular fracture surface of irradiated IN706, created by in situ straining at elevated temperatures, has been analyzed using AES. Large phosphorous enrichment (nearly 600 times the bulk concentrations) was observed on this fracture surface. Scanning and transmission electron microscopy indicate that the fracture path probably follows grain boundaries and precipitate-matrix interfaces, cutting through voids on both types of boundaries. Internal cracks, created during the initial tensile testing, could also have been present in the AES specimen. The resulting fracture surface, therefore, consists of grain boundaries, precipitate-matrix interfaces and void surfaces, as well as some regions of transgranular fracture.

All of these interfaces (except internal cracks from tensile testing) were exposed to neutron irradiation at 500°C. They were also exposed to postirradiation thermal cycling during the tensile testing, and during fracture in the AES system. The phosphorous segregation indicated in Figs. 11 and 12 could result from either the irradiation or the thermal exposure, or some combination of the two. As we previously mentioned, AES analysis of "as-irradiated" IN706 shows lower, but still significant, phosphorous enrichment on partially intergranular fracture surfaces.

The absence of helium release upon fracture is puzzling. Previous studies by Clausing and Bloom (11) and Sklad et al. (12) on alloys irradiated to similar fluences showed definite evidence of helium release. The possibility exists that any helium present in the alloy could have been lost during the tensile test; however, recent tests on hydrogen charged "as-irradiated" IN706 also did not show any helium release. This seems to leave only the possibility that the

helium is trapped elsewhere in the microstructure, and not released upon fracture. Determination of bulk helium levels in "as-irradiated" alloys should help to clarify this point.

Conclusions

The use of RGA and AES to study solute segregation to interfaces has been discussed, and experimental results on irradiated IN706 have been presented. AES results indicate that phosphorous segregation to internal interfaces takes place during irradiation at 500°C; however, the mechanism (irradiation-induced nonequilibrium segregation, irradiation-enhanced equilibrium segregation, or purely thermal segregation) cannot be deduced without appropriate control experiments.

The process of exposing internal interfaces for AES analysis must be given careful consideration in these experiments. The composition of intergranular (or interfacial) fracture surfaces produced during fracture at elevated temperature may not be entirely representative of "as-irradiated" interfaces. To the extent that changes occur after irradiation, but prior to separation of the interface, they, of course, may still be relevant to the fracture process. To the extent that segregation occurs to a fracture surface after it is exposed, it cannot be considered to have influenced the fracture process. For this reason, the ability to expose "as-irradiated" interfaces, without additional heating, seems highly desirable. Hydrogen charging is one promising way of doing this.

The complexity of the alloys, and the variety of interface types exposed for AES analysis, will also affect the extent to which experimental data can be interpreted. Clearly, experiments intended to explain mechanisms of fracture should concentrate initially on simple alloys where only grain boundaries, and possible void surfaces, are exposed for analysis.

While no helium release has been observed in IN706, the use of RGA for this purpose seems well established. Much work seems needed to determine the factors that influence whether or not helium will segregate to interfaces and influence mechanical behavior.

Finally, extrapolation of our knowledge about unirradiated alloys suggests that segregation may strongly affect the behavior of irradiated alloys; however, clear demonstration of a cause-and-effect relationship is far from established. In general, other irradiation-induced effects such as hardening, void formation at interfaces, and alterations of precipitate-free zones can be expected to act in combination with segregation to produce a net loss in ductility.

Acknowledgments

The authors wish to thank colleagues at ORNL for their contributions to various phases of this work. These include L. Heatherly and R. Padgett for assistance in conducting Auger analysis, L. Schrader for scanning microscopy of fracture surfaces, P. S. Sklad for transmission electron microscopy, and A. F. Rowcliffe for useful discussions. The assistance of F. A. Scarboro and S. P. Buhl in preparation of the manuscript is also gratefully acknowledged.

References

1. J. H. Westbrook and S. Floreen, "Grain Boundary Segregation and the Grain Size Dependence of Strength of Nickel-Sulfur Alloys," Acta Met. 17 (1969) 1175.

2. M. G. Lozinskiy, G. M. Volkogon, and N. Z. Pertsovskiy, "Investigation of the Influence of Zirconium Additions on the Ductility and Deformation Structure of Nickel Over a Wide Temperature Range," Russian Metallography 5 (1967) 65.

3. C. L. White and D. F. Stein, "Sulfur Segregation to Grain Boundaries in in Ni_3Al and $Ni_3(Al,Ti)$ Alloys," Met. Trans. 9A (1978) 13.

4. E. D. Hondros, "The Influence of Phosphorous in Dilute Solid Solution on the Absolute Surface and Grain Boundary Energies of Iron," Proc. Roy. Soc. London A 286 (1965) 479.

5. M. P. Seah, "Segregation and the Strength of Grain Boundaries," Proc. Roy. Soc. London A 349 (1976) 535,

6. W. Losch, "Temper Embrittlement and Surface Segregation, an AES and ILS Study," Acta Met. 27 (1979) 567.

7. A. Joshi and D. F. Stein, "An Auger Spectroscopic Analysis of Bismuth Segregated to Grain Boundaries in Copper," J. Inst. Metals 99 (1971) 178.

8. E. D. Hondros and D. McLean, "Cohesion Margin of Copper," Phil. Mag. 29 (1974) 771.

9. L. K. Mansur and W. G. Wolfer, A Study of the Effect of Void Surface Coatings on Radiation-Induced Swelling, ORNL/TM-5670 (1977). Available from NTIS, U.S. Department of Commerce, Springfield, VA 22161

10. P. R. Okamoto and L. E. Rehn, "Radiation-Induced Segregation in Binary and Ternary Alloys," J. Nucl. Mater. 83(1), 2 (1979).

11. R. E. Clausing and E. E. Bloom, "Auger Electron Spectroscopy of Fracture Surfaces in Irradiated Type 304 Stainless Steel," Proceedings Fourth Bolton Landing Conference, J. Walters, et al., eds. (1974), p. 491.

12. P. S. Sklad, R. E. Clausing, and E. E. Bloom, "Effects of Neutron Irradiation on Microstructure and Mechanical Properties of Nimonic PE-16," ASTM-STP 61 (1976), p. 139.

13. Calvin L. White, Robert E. Clausing, and Lee Heatherly, "The Effect of Trace Element Additions on the Grain Boundary Composition of Ir + 0.3 Pct W Alloys," Met. Trans. A, 10A (1979) 683.

Fig. 1. Free energy of vacancy cluster formation versus cluster size for two values of surface energy. (L. K. Mansur and W. G. Wolfer, ORNL-TM 5670).

Fig. 2. Schematic illustrating qualitatively three mechanisms for irradiation-induced solute segregation.

Fig. 3. Top view of the Auger system used at ORNL.

Fig. 4. Elevation view of the Auger straining stage with a specimen in place.

Fig. 5. Specimen, specimen holder, and one-half of specimen holder containing fractured specimen for Auger analysis of fracture surface.

Fig. 6. Microstructure of unirradiated Inconel 706 in the STA condition.

Fig. 7. Microstructure of Inconel 706 STA irradiated to 5×10^{22} n cm^{-2} at 500°C and tested at 610°C.

Fig. 8. Fracture surface of A_3 magnified 100×.

Fig. 9. Portion of A_3 fracture surface magnified 1000×.

Fig. 10. Portion of fracture surface shown in Fig. at a magnification of 5000×.

Fig. 11. Auger spectra obtained by rastering 4 keV electron beam over ½ A_3 fresh fracture surface.

Fig. 12. Auger spectra obtained by rastering 4 keV electron beam over the same area as in Fig. 11 following 5 min sputtering with argon ions at 1 kV.

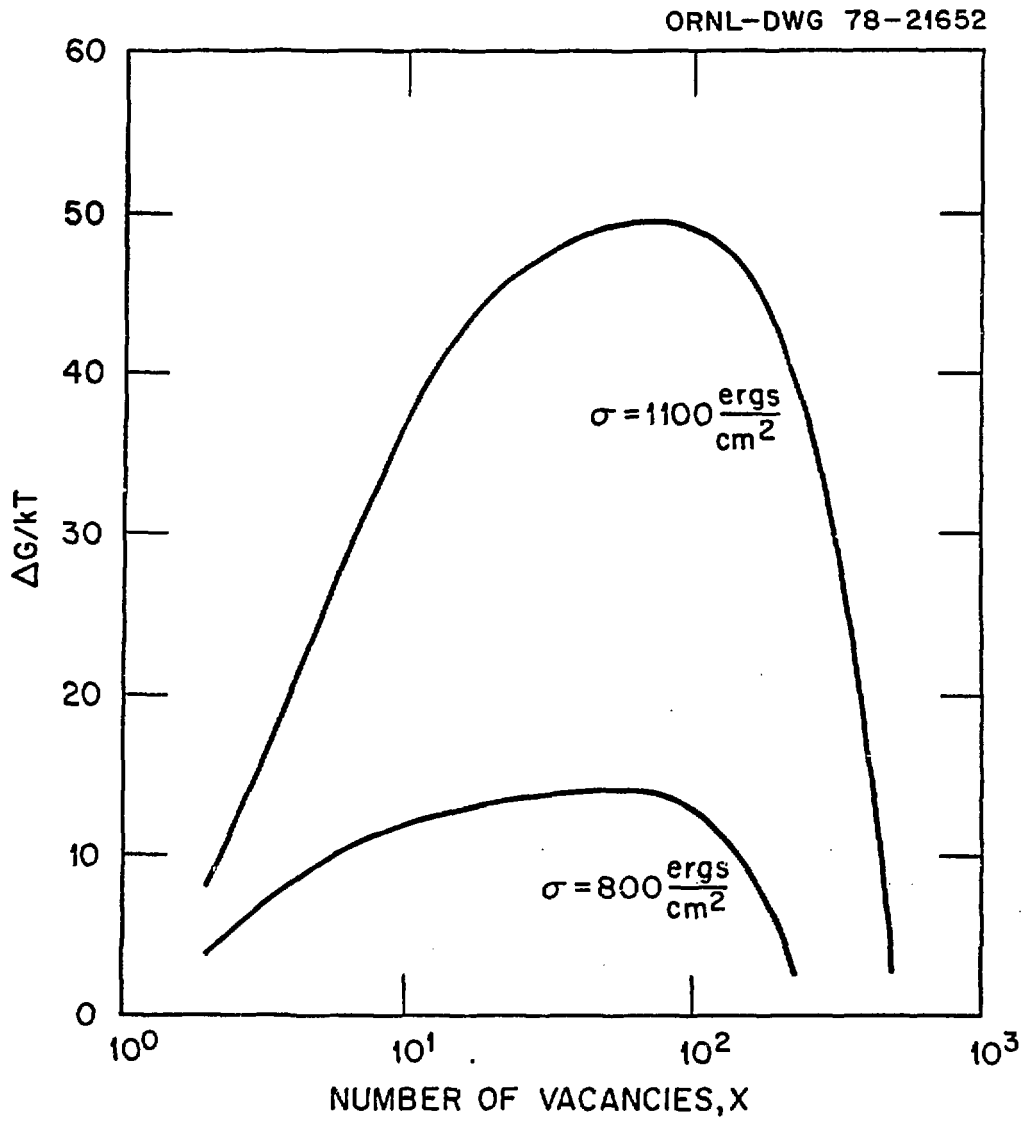

Fig. 1. Free energy of vacancy cluster formation versus cluster size for two values of surface energy. (L. K. Mansur and W. G. Wolfer, ORNL-TM 5670).

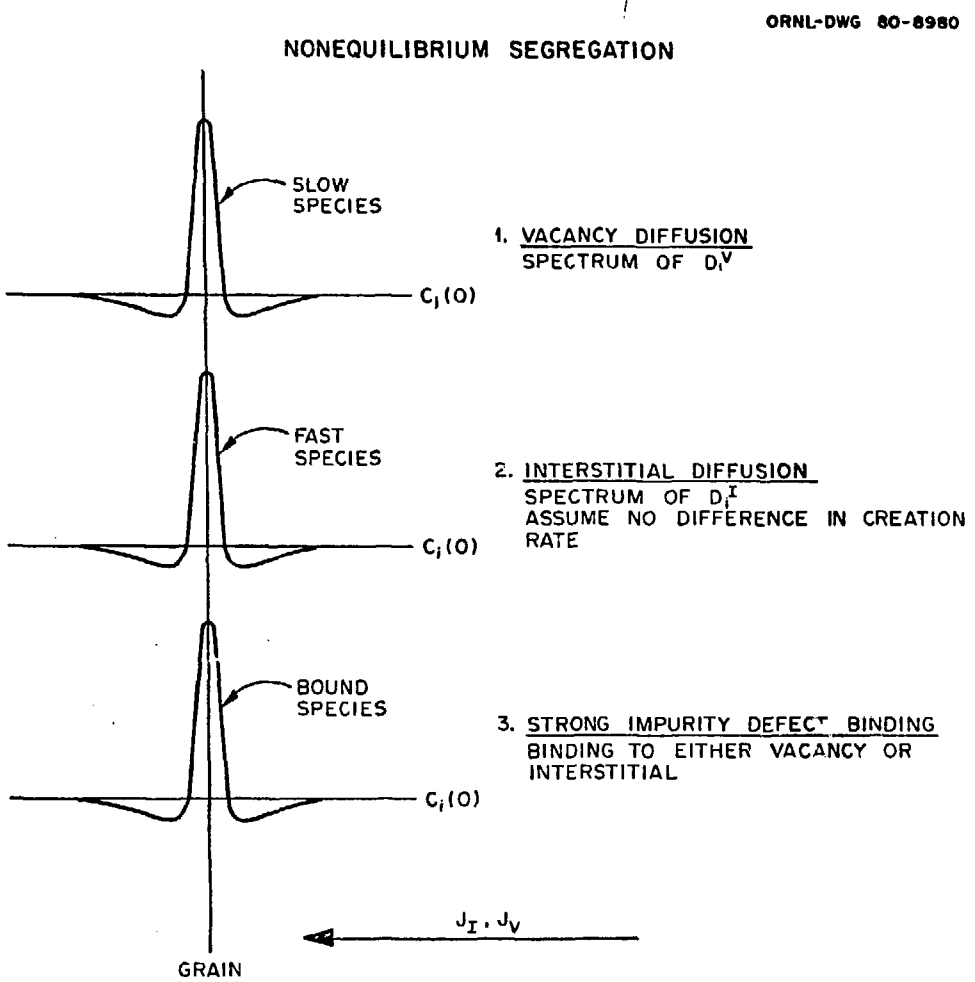

Fig. 2. Schematic illustrating qualitatively three mechanisms for irradiation-induced solute segregation.

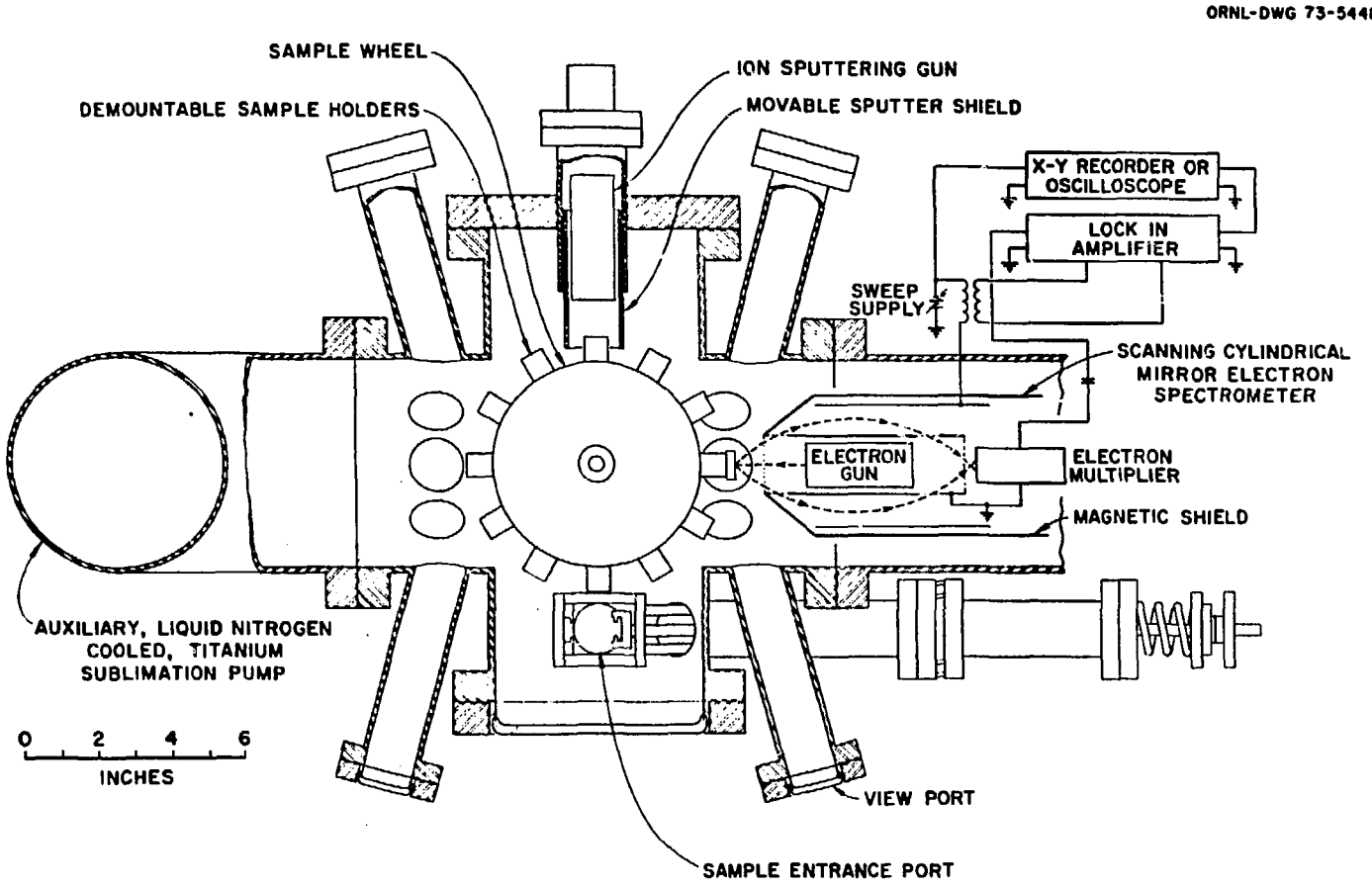

Fig. 3. Top view of the Auger system used at ORNL.

ORNL-DWG 73-5140

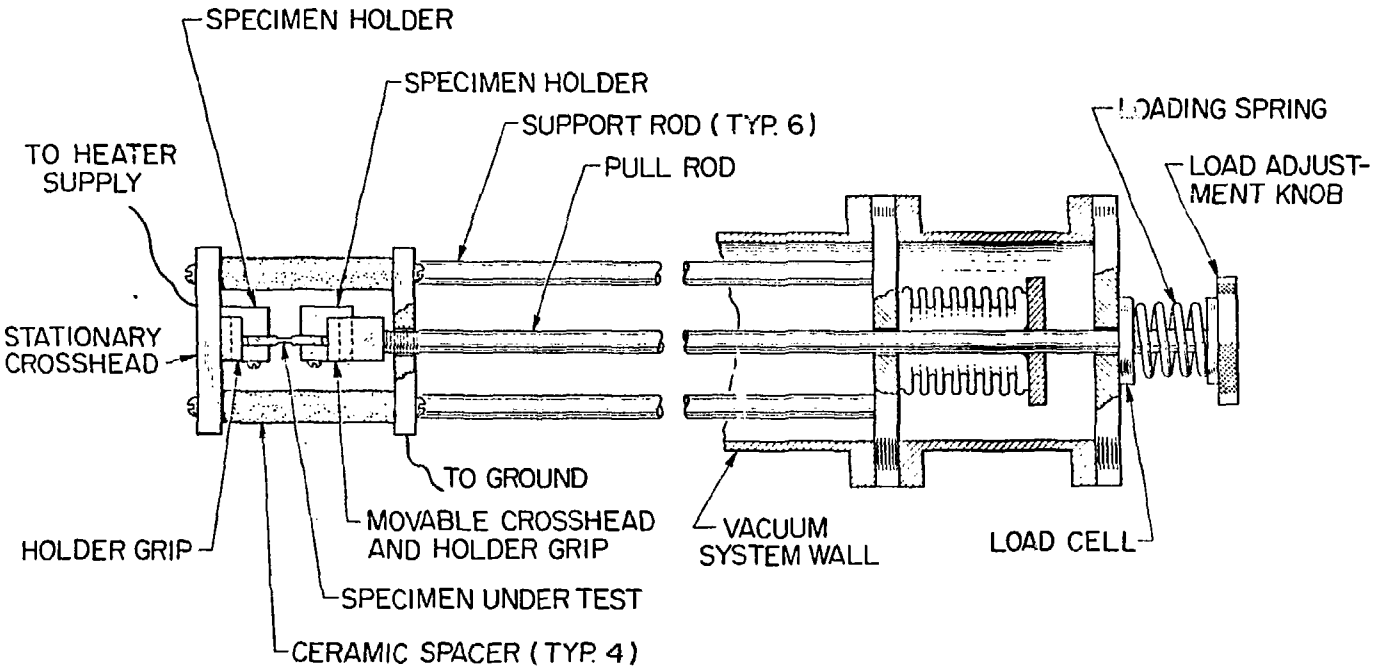

Fig. 4. Elevation view of the Auger straining stage with a specimen in place.

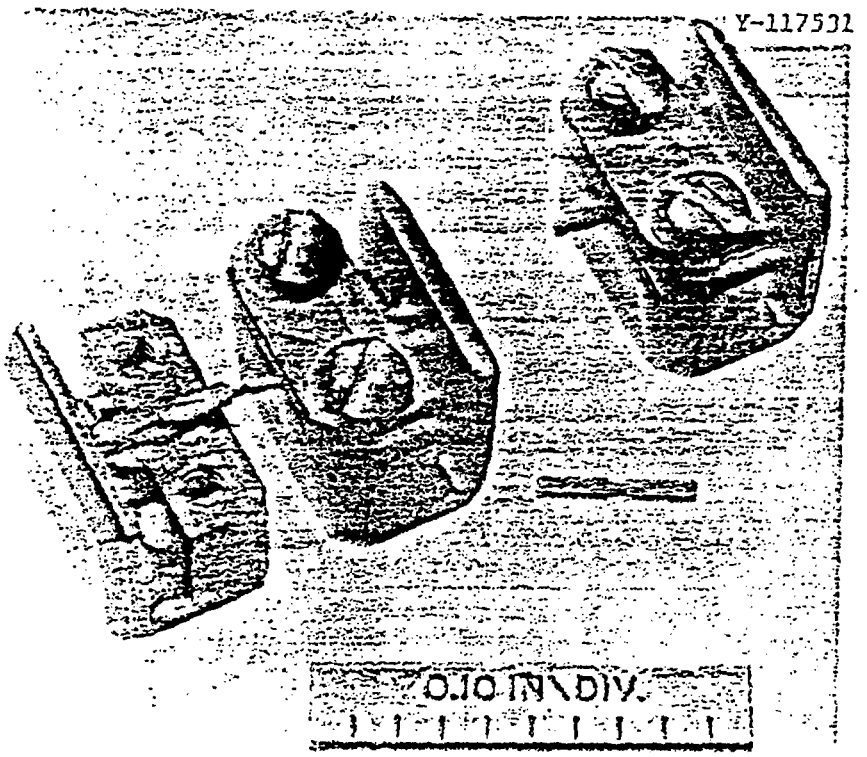

Fig. 5. Specimen, specimen holder, and one-half of specimen holder containing fractured specimen for Auger analysis of fracture surface.

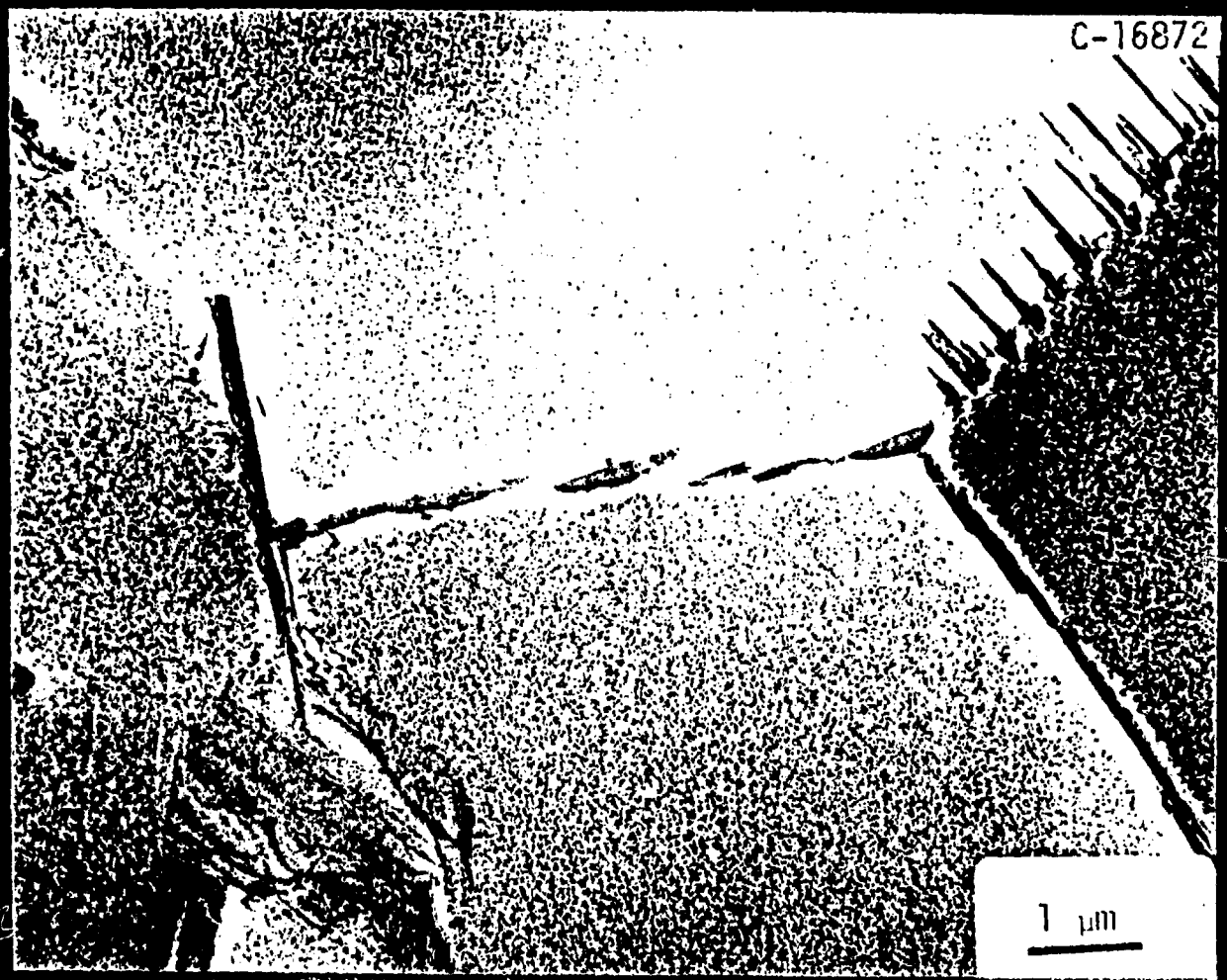

Fig. 6. Microstructure of unirradiated Inconel 706 in the STA condition.

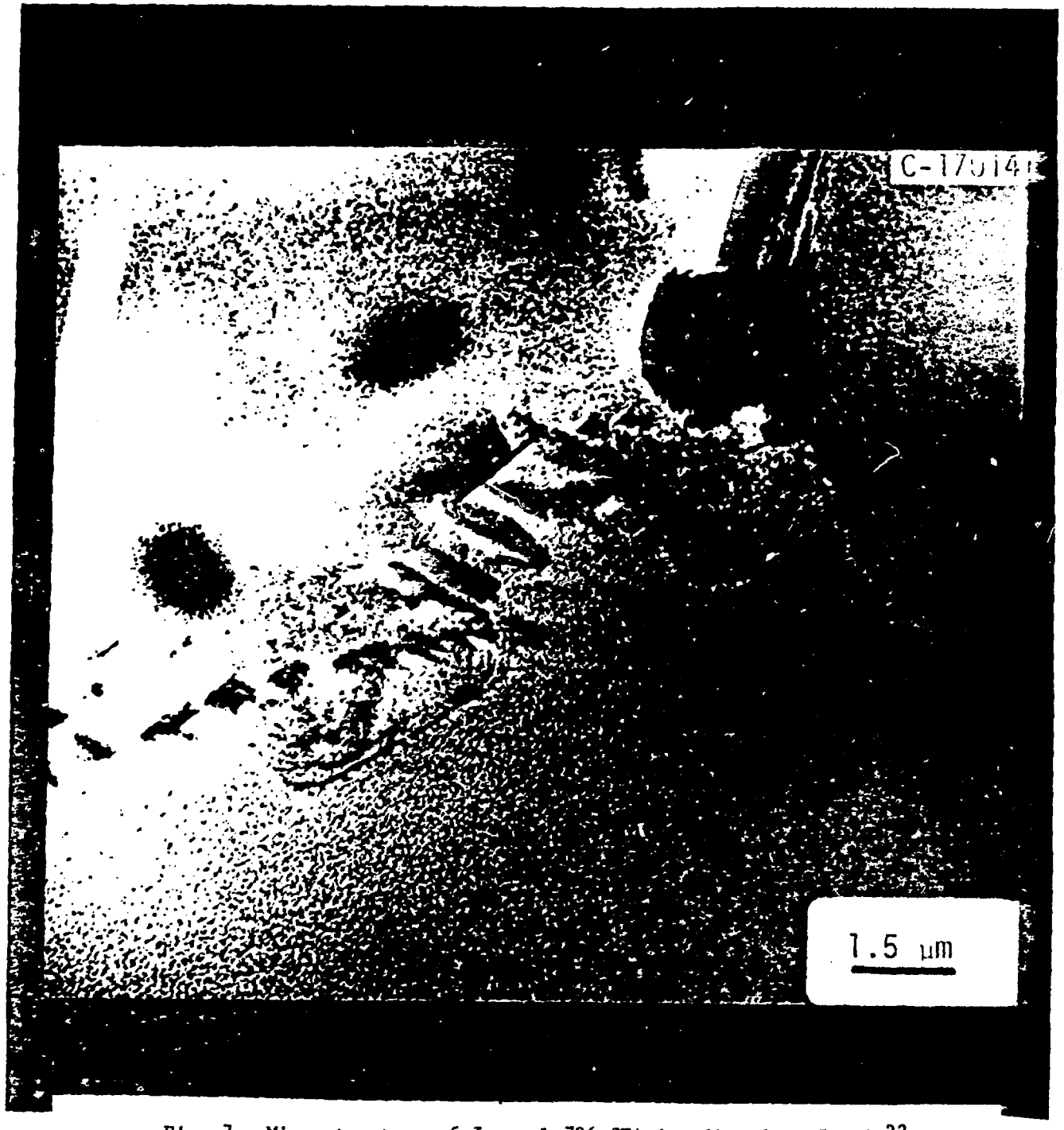

Fig. 7. Microstructure of Inconel 706 STA irradiated to 5×10^{22} n cm^{-2} at 500°C and tested at 610°C.

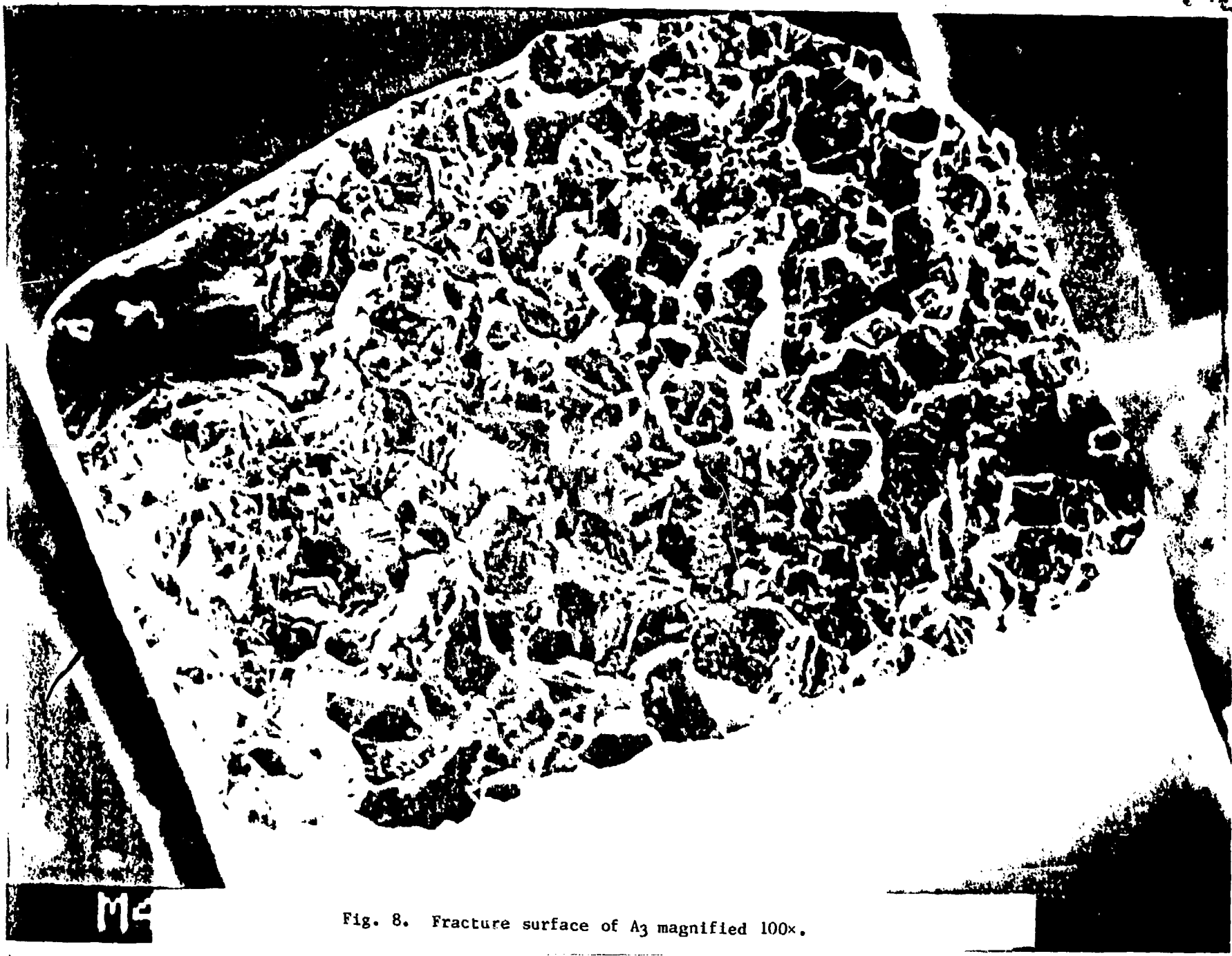

Fig. 8. Fracture surface of A_3 magnified 100×.

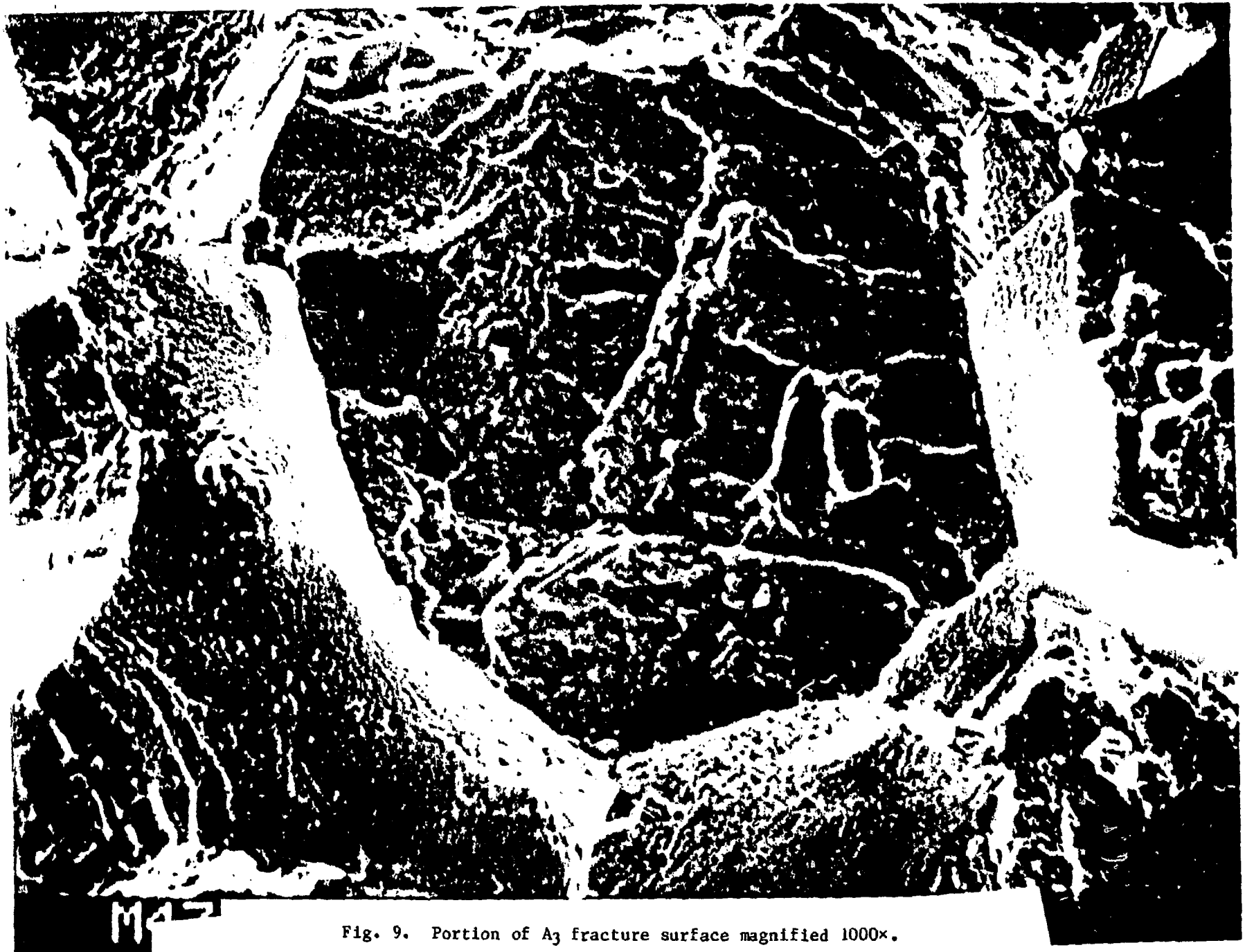

Fig. 9. Portion of A_3 fracture surface magnified 1000×.

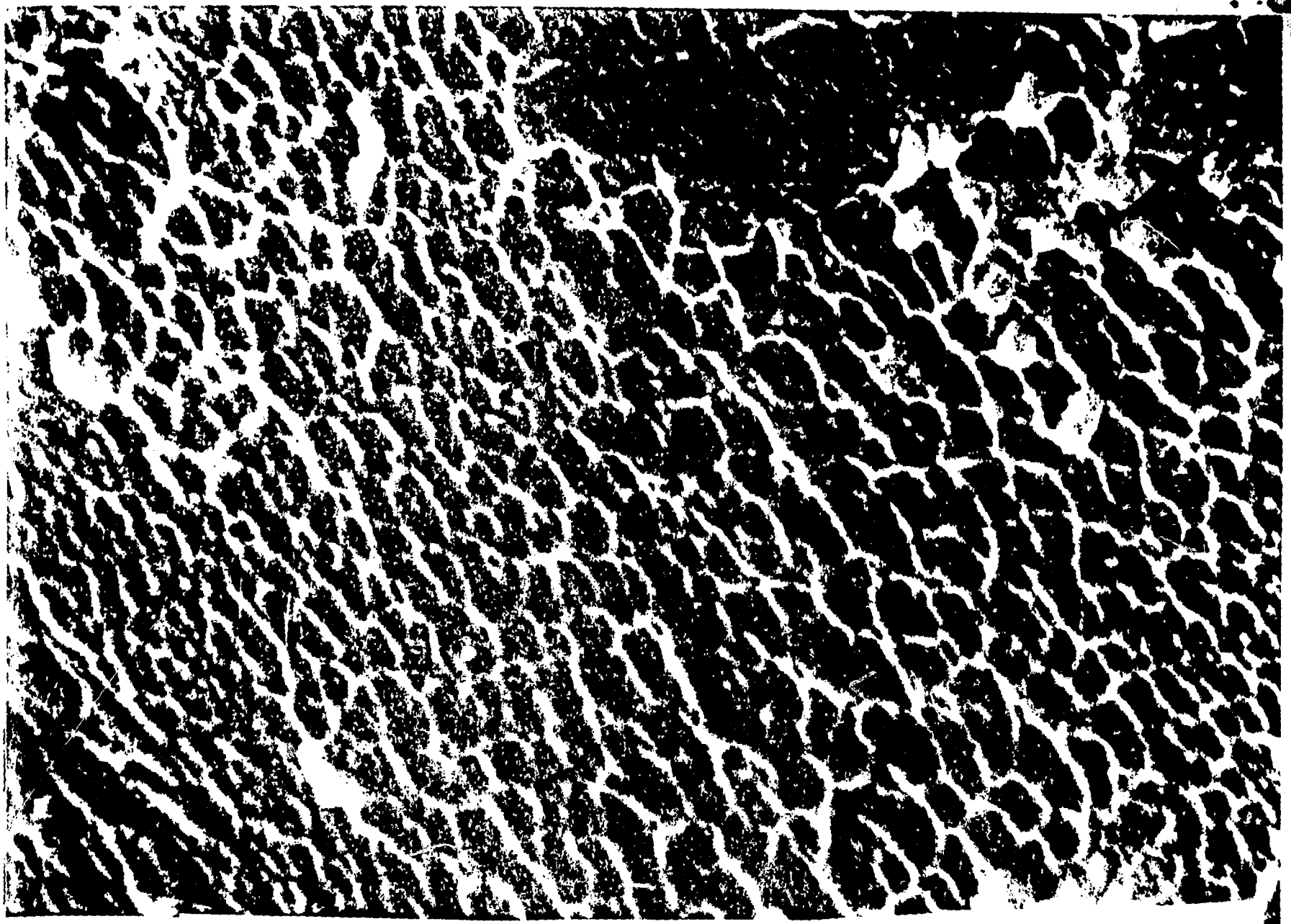

Fig. 10. Portion of fracture surface shown in Fig. at a magnification of 5000×.

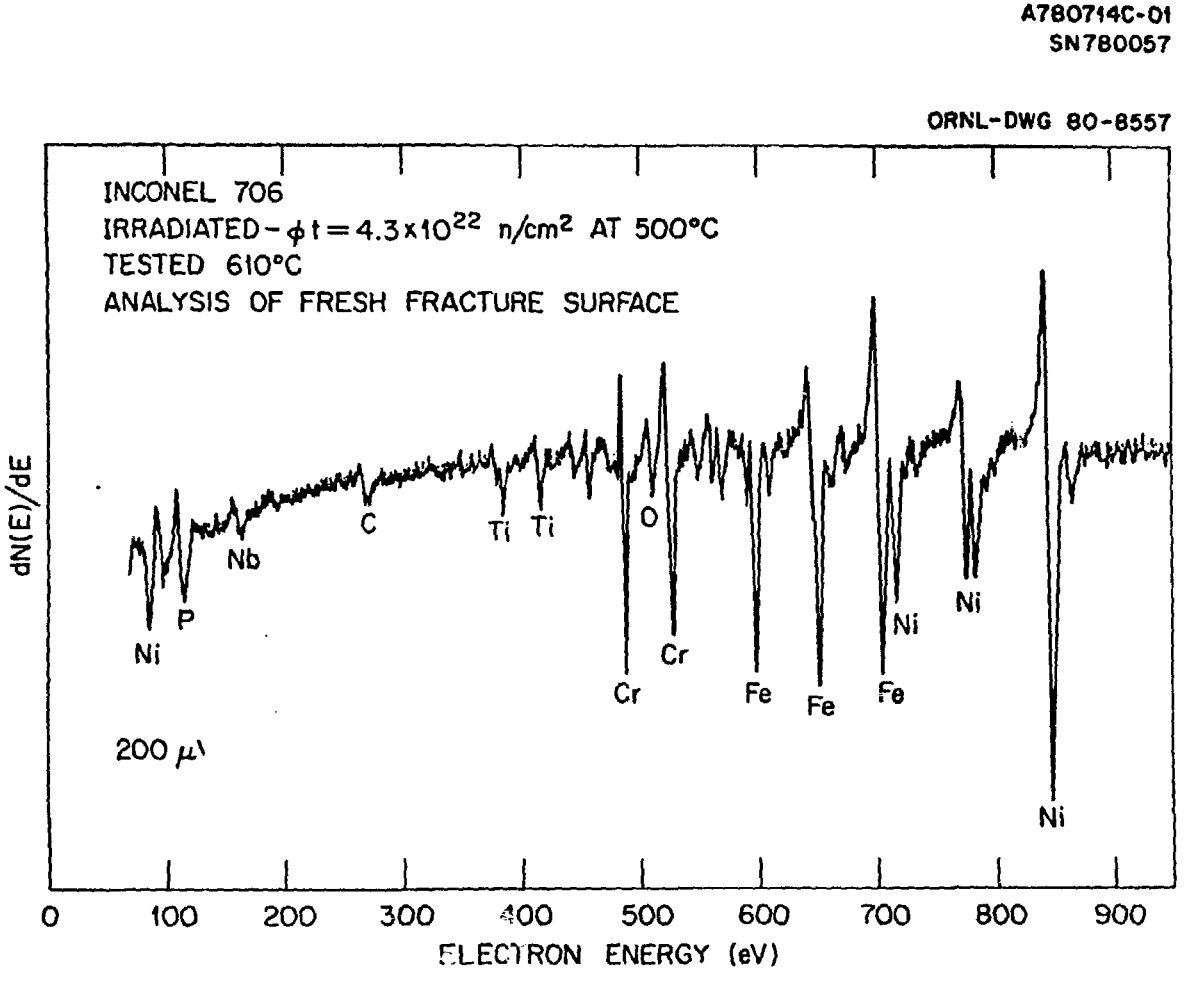

Fig. 11. Auger spectra obtained by rastering 4 keV electron beam over 1/2 A_3 fresh fracture surface.

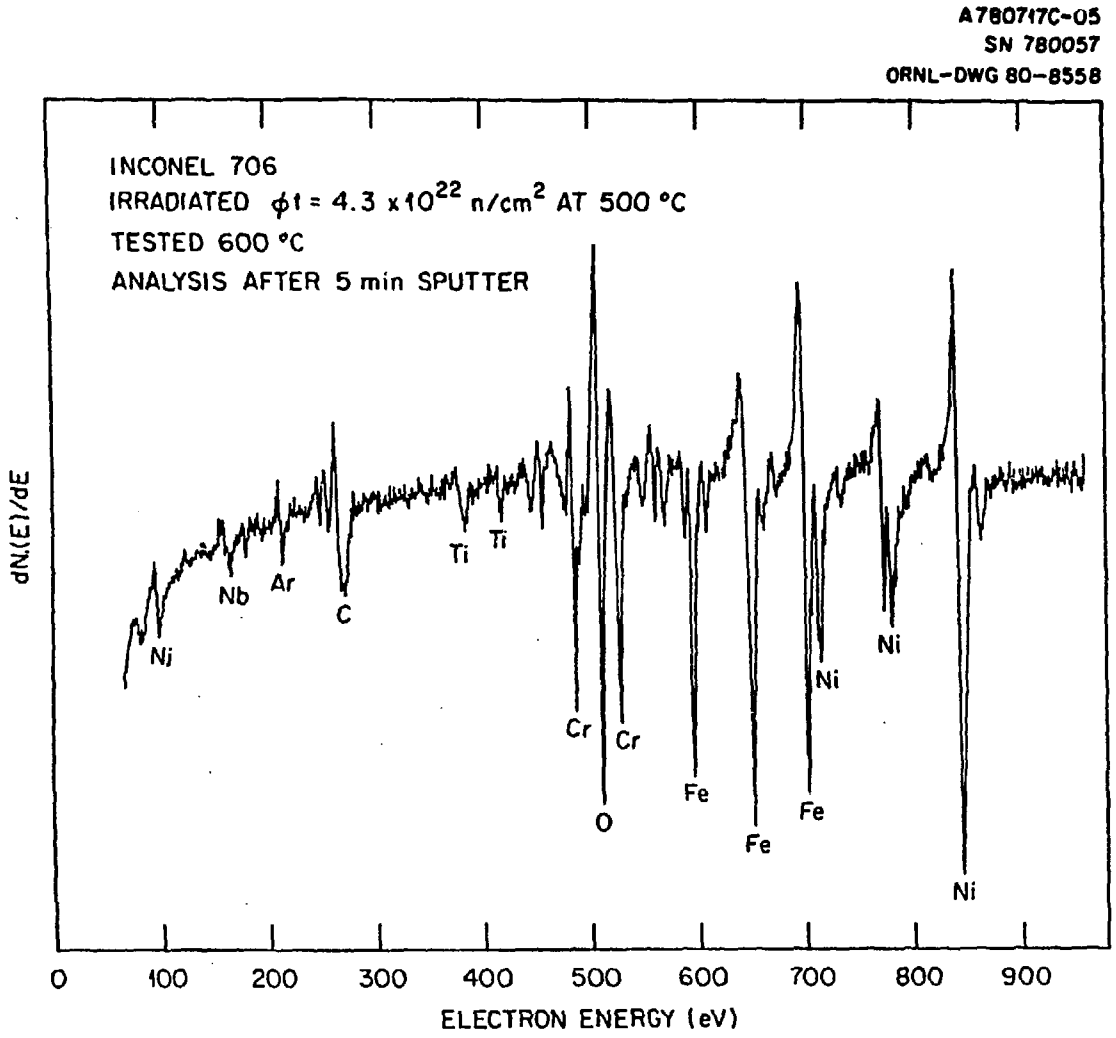

Fig. 12. Auger spectra obtained by rastering 4 keV electron beam over the same area as in Fig. 11 following 5 min sputtering with argon ions at 1 kV.